Evolution of Dust Clouds in Afterglow Plasmas

John K. Meyer and Robert L. Merlino

***Abstract*— The observations of the evolution of dust clouds in afterglow plasmas at various neutral pressures are presented. Four cases were studied which showed a large variation in the cloud dynamics. In two cases, the clouds responded by rapidly shedding an outer layer of dust. In another case, the entire cloud exhibited a nearly uniform expansion—Coulomb explosion. In perhaps the most exotic case, the cloud splits into two clouds—Coulomb fission. The results for the case of the Coulomb expansion were compared with a theoretical model that included the effects of neutral drag.**

***Index Terms*— Coulomb explosion, Coulomb fission, dusty plasma.**

I. Introduction

OFTEN, the physics of complex systems can be investigated by observing those systems under extreme conditions. The response of a system when its external conditions are suddenly changed may reveal aspects of the interactions between the constituents that might not otherwise be accessible in the quiescent state. This method has been used to study the physics of small, charged dust clusters in a dusty or complex plasma. Here, the observations are presented of the dynamical evolution of clusters of 1-μm-diameter charged silica microspheres suspended in a dc glow discharge argon plasma when the plasma was suddenly turned OFF.

A few experiments have investigated the Coulomb explosion of a cluster of dust particles in an afterglow plasma. A Coulomb explosion occurs when the loss of plasma occurs on such a rapid timescale that the shielding of the particles is greatly reduced, while the dust particles retain a substantial residual charge. Barkan and Merlino [1] observed the explosion of a nearly spherical cluster of dust particles confined in an anode glow discharge formed on the endplate of a Q machine plasma. The magnitude of the dust particle acceleration obtained from a molecular dynamics (MD) simulation [2] was in agreement with the value observed in the experiment. A nearly uniform explosion of the dust particles occurred when the anode voltage was suddenly turned OFF. Filatova *et al.* [3] observed the decay of dust structures in an RF discharge at a neutral pressure $P_n = 100$ Pa, after the discharge was switched OFF. Antonova *et al.* [4] used a novel RF discharge device ($P_n \sim 30$–100 Pa) with a lower grounded electrode that contained an additional RF-driven central segment. A localized plasma spot was produced above this segment which confined a dense cloud of dust particles deep in the plasma sheath. When the voltage to the additional segment was turned OFF, the dense cloud of dust particles exploded into the main plasma. Particle velocities of approximately tens of millimeters per second were measured and compared with the results of a particle-in-cell simulation and simple theoretical analyses. Experiments have been performed to specifically study the decharging of dust in the afterglow plasmas [5]–[7]. The observations of [5] were performed under microgravity conditions on the International Space Station in the plasma crystal experiment-Nefedov laboratory. A detailed analysis of the kinetics of the plasma decay, relaxation of the electron temperature, and dust charge variation was reported in [6]. The analysis of dust cluster explosions (or expansions) has been performed using both the analytical theory [8] and the MD simulations [2], [9].

In Section II, the experimental device and diagnostics are described. The observations are presented in Section III. A discussion and summary of the results are given in Section IV.

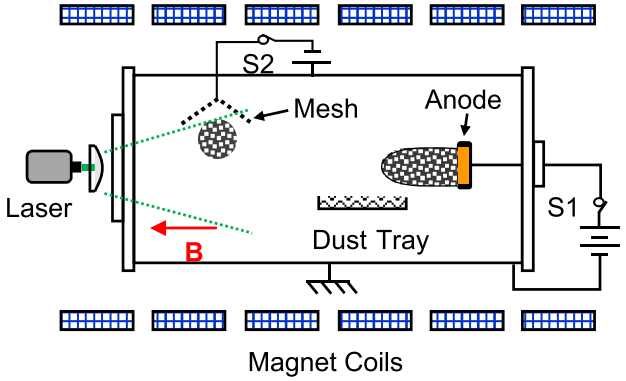

Fig. 1. Schematic of the experimental device.

II. Experimental Device

The experimental device is schematically shown in Fig. 1. The device consists of a grounded stainless-steel cylindrical vacuum chamber, 60 cm in diameter and 1 m in length. A dc glow discharge is ignited using a 3.4-cm-diameter anode disk, biased to +250 V, in a background of argon gas at pressures in the range $P_n \sim 100$–200 mTorr. The discharge current for all the cases studied was $I_d = 5$ mA. An axial magnetic field of 3 mT is applied to provide confinement of the electrons. The plasma density and electron temperature are measured using a double Langmuir probe, and an emissive probe is used to obtain the plasma potential profiles. The

Manuscript received July 31, 2015; revised November 13, 2015; accepted November 25, 2015. Date of publication December 17, 2015; date of current version April 8, 2016. This work was supported by the U.S. Department of Energy under Grant DE-FG02-04ER54795. *(Corresponding author: Robert L. Merlino.)*

The authors are with the Department of Physics and Astronomy, The University of Iowa, Iowa City, IA 52242 USA (e-mail: jkmeyer54@gmail.com; robert-merlino@uiowa.edu).

This paper has supplementary downloadable material available at http://ieeexplore.ieee.org., provided by the author.

Color versions of one or more of the figures in this paper are available online at http://ieeexplore.ieee.org.

Digital Object Identifier 10.1109/TPS.2015.2504920

plasma density is in the range $n_i \sim 10^{12}$–10^{13} m^{-3}, and the electron temperature $T_e \sim 2$–4 eV. The argon ions are assumed to be at room temperature.

Monodisperse, silica microspheres (nominal radius $a = 0.5$ μm and mass $m_d \sim 10^{-15}$ kg) located on a tray below the anode were incorporated into the anode glow during startup. The dust charge was estimated to be $q_d \sim -2000e$, using the orbital motion-limited theory for $T_e \sim 100T_i \sim 2.5$ eV. The dust cloud was illuminated using 532-nm laser light that was spread into a vertical sheet using a cylindrical lens. The laser and lens were located far from the dust cloud, so that a large sheet of laser light of nearly uniform intensity illuminated the full space well above and below the dust cloud. The cloud was imaged using a 1000 pixel by 1000-pixel CMOS Photron Fastcam at frame rates up to 2000 frames/s. The gray-scale image intensities are proportional to the dust density. Dust densities were in the range $n_d \sim 10^{10}$–10^{11} m^{-3}. The dust densities were estimated by counting individual dust particles within a known volume.

An additional conical mesh electrode was used to draw dust from the main plasma to form a small suspended dust cluster. The mesh was either grounded or biased from -10 to -50 V. Once a suitable secondary dust cloud was formed, an electronic switch was used to simultaneously disconnect the bias of both the anode and the mesh, leaving both electrically floating. When the mesh and anode were switched to floating, the plasma was extinguished and the confining forces on the secondary cloud were eliminated. The dynamical evolution of the dust cloud was then recorded as a sequence of video images.

III. Observations

We will present the observations of the evolution of four dust clouds that were confined in a plasma which was suddenly turned OFF. It is important to point out that, unlike observations of a steady state dust cloud, we are dealing in each case with a different cloud, since each cloud is necessarily destroyed in the experiment. Although we have control over some of the external conditions in the experiment, mainly the pressure and discharge current, each trapped cloud is unique, in that the shape, size, dust distribution, and number of particles are different. The mesh voltage, V_m, was adjusted to try to form clouds of similar shape and sizes as the pressure was varied. However, we found that the initial mesh potential had little effect on the evolution of the dust clouds after the bias was turned OFF. As will be evident, clouds formed under nominally similar conditions may exhibit very different dynamical evolutions when released. We have investigated the evolution of dozens of dust clouds and will present the results of a subset, chosen to illustrate the variety of responses that are apparently possible. The evolution of each cloud was recorded at 2000 frames/s, or 0.5 ms between video frames. We point out that while the dust clouds were 3-D, only 2-D observations of the clouds using a vertical laser sheet were performed.

Video clips (audio video interleave format) of the four cases studied are included as supplementary material, which is available at http://ieeexplore.ieee.org.

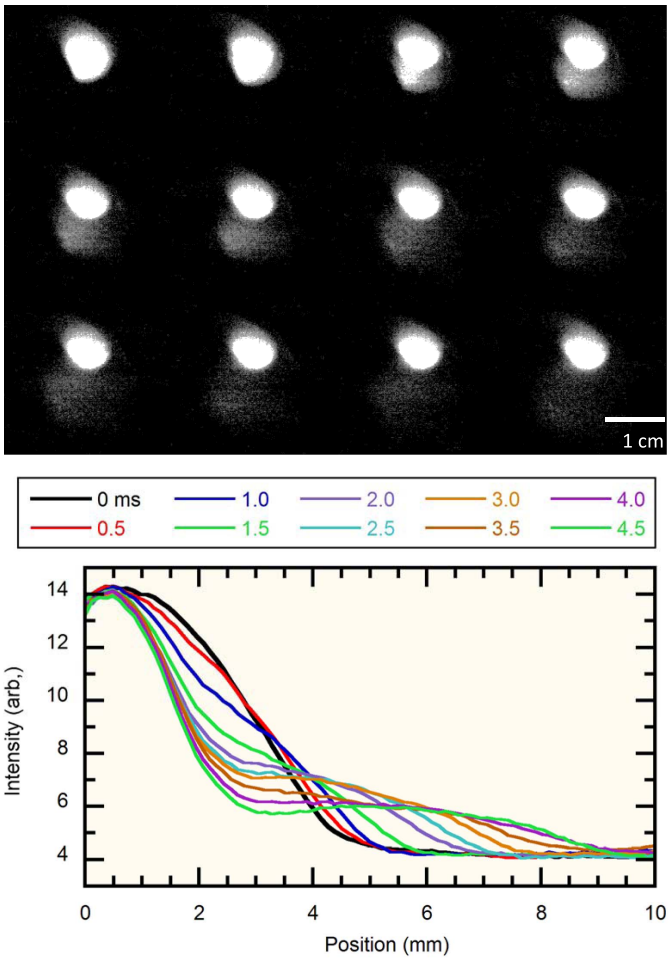

Fig. 2. Top: montage of single-frame video images (see supplementary material for video clip of Case 1) of expanding dust cloud at $P_n = 150$ mTorr in 1-ms time intervals, left to right and top to bottom. Bottom: gray-scale intensity profiles along a vertical line through the dust cloud images at indicated times following the release of the cloud at $t = 0$.

A. Case 1: $P_n = 150$ mTorr (20 Pa), $I_d = 5$ mA, and $V_m = -20$ V

Fig. 2 (top) shows a montage of single-frame images of the evolution of the dust cloud after the mesh and anode bias voltages were switched OFF at $t = 0$. The images are in 1-ms steps proceeding left to right and top to bottom. The initial cloud ($t = 0$) is roughly 12-mm long and 8-mm wide, and elliptically shaped. For $t > 0$, the lower 1/3 of the cloud's outer layer was blown off and expanded as it moved downward. The U-shaped blow-off layer was located initially below the part of the cloud with the highest dust density. Profiles of the gray-scale intensity of the scattered light along a vertical line through the center of the cloud in 0.5-ms time steps are shown in Fig. 2 (bottom). These profiles show the gradual erosion of the outer portion of the bottom of the cloud which moves downward and expands as it separated from the main cloud.

B. Case 2: $P_n = 200$ mTorr (20 Pa), $I_d = 5$ mA, and $V_m = 0$ V

The montage of single-frame images at 1-ms intervals for this case is shown in Fig. 3. The cloud in this case was

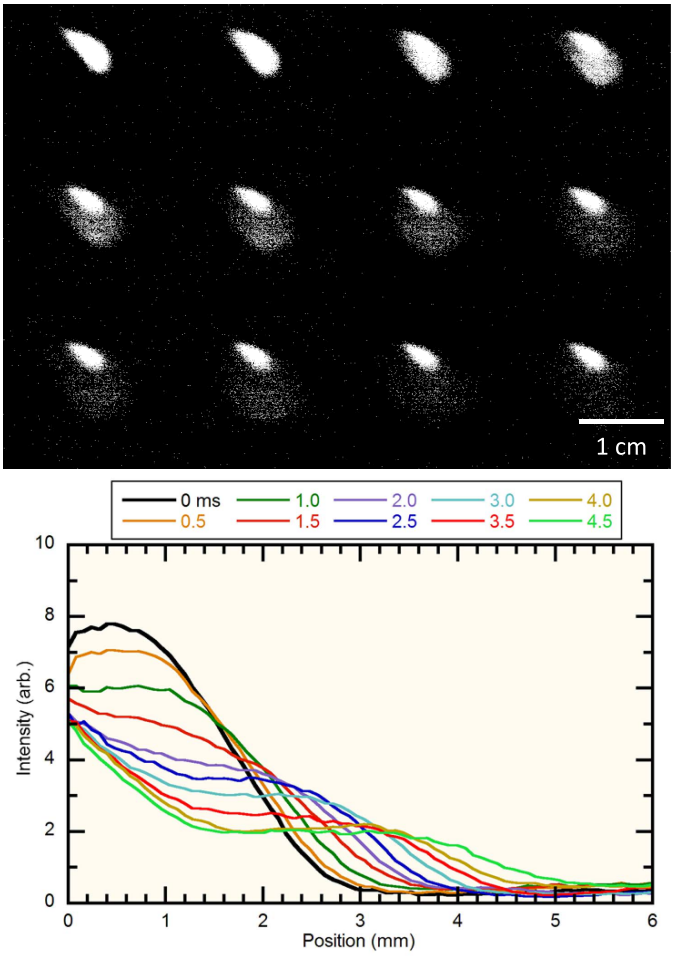

Fig. 3. Top: montage of single-frame video images (see supplementary material for video clip of Case 2) of expanding dust cloud at $P_n = 205$ mTorr in 1-ms time intervals, left to right and top to bottom. Bottom: gray-scale intensity profiles along a vertical line through the dust cloud images at indicated times following the release of the cloud at $t = 0$.

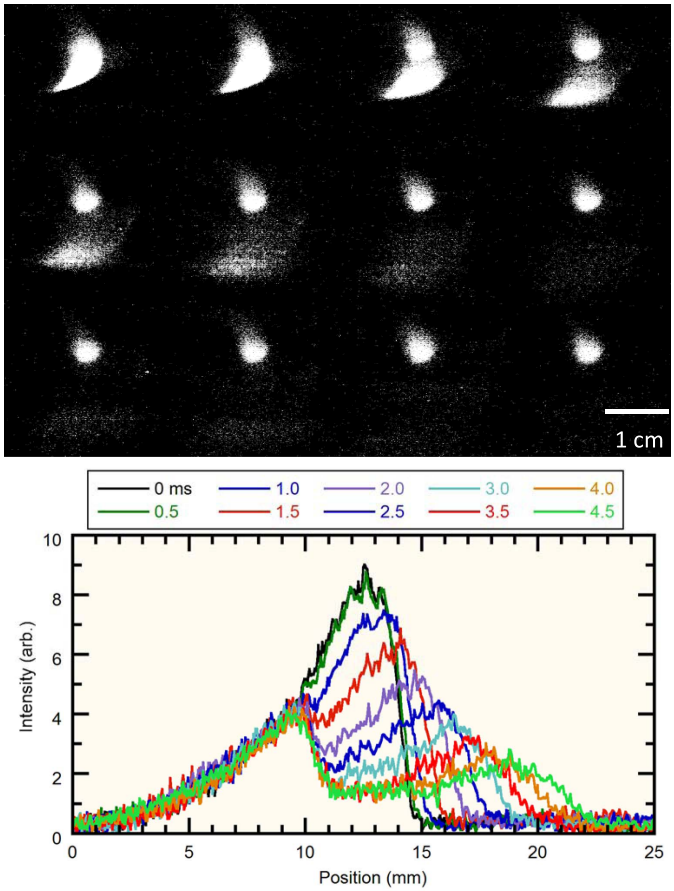

Fig. 4. Top: montage of single-frame video images (see supplementary material for video clip of Case 3) of a dust cloud undergoing Coulomb fission at $P_n = 100$ mTorr in 1-ms time intervals, left to right and top to bottom. Bottom: gray-scale intensity profiles along a vertical line through the dust cloud images at indicated times following the release of the cloud at $t = 0$.

6-mm long by 3.3-mm wide, somewhat smaller than in Case 1, and crescent-shaped as opposed to elliptical. The cloud evolution in this case was similar to Case 1, except that a larger portion of the outer layer of this cloud separates from the main smaller cloud. The cloud expanded nearly uniformly as it separated. Light intensity profiles taken along a vertical line through the cloud center are shown in Fig. 3 (bottom). In this case, the main cloud was eroded as the larger outer layer separated. The separation speed was somewhat lower in this case.

C. Case 3: $P_n = 100$ mTorr (13 Pa), $I_d = 5$ mA, and $V_m = -50$ V

This was perhaps the most unusual case that was observed. The montage of single-frame images at 1-ms intervals is shown in Fig. 4. In this case, the cloud was crescent-shaped, 18-mm long by 6-mm wide. The cloud responded to the switching OFF of the anode and mesh bias voltages by splitting into two pieces—Coulomb fission. The lower fragment of 9-mm height splits off from a smaller upper fragment of 5-mm height. The lower fragment separated from the upper cloud at an average speed of 5 m/s over the first 1 ms. Vertical profiles of the light intensity obtained from the single-frame video images are shown in Fig. 4 (bottom). The lower fragment expanded as it moved downward, while the upper fragment was approximately stationary, until it eventually began to fall under the influence of gravity and neutral drag.

D. Comparison of Cloud Dynamics for Cases 1–3

Fig. 5(a) shows the variation of the position of the bottom edge of the clouds with time for Cases 1–3. The corresponding velocities obtained from Fig. 5(a) are shown in Fig. 5(b). The maximum rates of separation or fragmentation of the clouds for $P_n = 100$, 150, and 200 mTorr were, respectively, 1.8, 0.9, and 0.6 m/s. The rates of separation decreased with increasing neutral pressure. Most of the acceleration occurred in the first 2 ms, with magnitudes of 900, 450, and 300 m/s^2 at $P_n = 100$, 150, and 200 mTorr, respectively.

E. Case 4: $P_n = 200$ mTorr (26 Pa), $I_d = 5$ mA, and $V_m = 0$ V

Unlike Cases 1 and 2, which showed a rapid blow-off of the outer portion of the cloud, or Case 3, which showed a

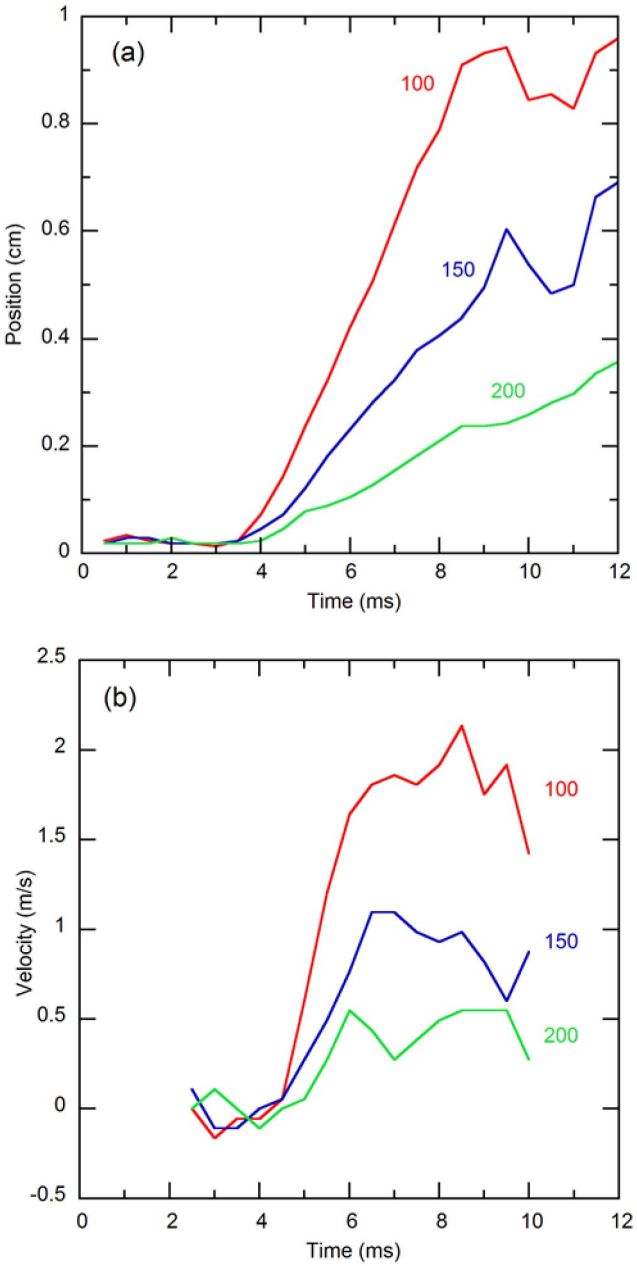

Fig. 5. (a) Variation of the position of the bottom of the clouds shown in Figs. 2–4, with time. (b) Variation of the velocity of the bottom of the clouds shown in Figs. 2–4, with time, obtained from (a).

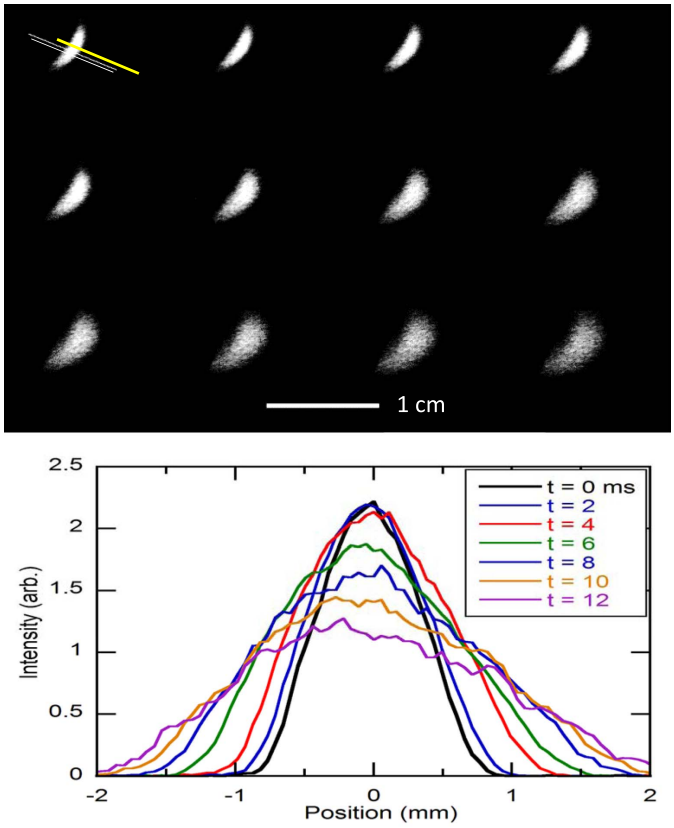

Fig. 6. Top: montage of single-frame video images (see supplementary material for video clip of Case 4) of a dust cloud undergoing Coulomb expansion at $P_n = 200$ mTorr in 1-ms time intervals, left to right and top to bottom. Bottom: gray-scale intensity profiles along a vertical line through the dust cloud images at indicated times following the release of the cloud at $t = 0$.

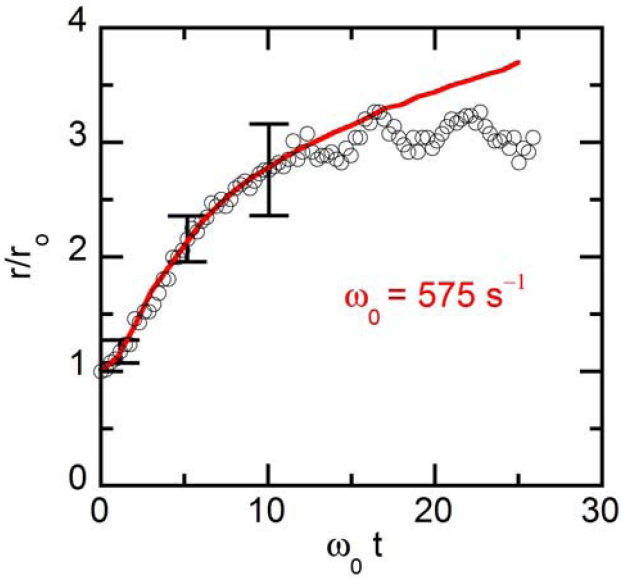

Fig. 7. Circles: experimental data showing the variation of the cloud radius r/r_o normalized to its initial value, r_o with $\omega_o t$. Solid curve: results of the numerical solution to (1) for $\gamma = 330$ s^{-1} and $\omega_o = 575$ s^{-1}.

fragmentation or fission of the cloud, Case 4 provided an example of a cloud that remained intact as it expanded roughly uniformly in both the vertical and horizontal directions. The cloud in this case was crescent-shaped, 8-mm long and 2-mm wide. The 1-ms time step montage of the expansion of this cloud is shown in Fig. 6. The cloud expanded for roughly 15 ms, roughly doubling in size, and fell downward. Light intensity profiles measured across the line indicated in the first image of the montage are shown in Fig. 6 (bottom). The maxima of the light intensity profiles for each time were shifted to zero to show the expansion more clearly. The profiles were fitted to a Gaussian function, and the radius of the cloud was obtained from the full width at half maximum of the profiles. The area under the curves in Fig. 6 was approximately the same indicating that the expansion was mostly radial. The normalized cloud radius, r/r_o, where r_o is the radius at $t = 0$, is plotted in Fig. 7 versus $\omega_0 t$, where ω_0 is a normalization

parameter that will be defined in Section IV. The cloud expansion occurs to $\omega_0 t \approx 10$, after which the expansion slows down and reaches a final value $r/r_o \sim 3$. Fig. 7 (solid curve) shows the result of a theoretical model which will be discussed in Section IV.

IV. Discussion and Summary

We have presented observations showing the evolution of dust clouds under various conditions when the plasma and confining forces were removed. A key point to emphasize is that, due to the different time scales involved in this process, the dust particles may retain a substantial charge after the plasma has decayed. The unconfined dust cloud then evolves dynamically under either a bare Coulomb repulsion force between the particles, or a shielded (Yukawa) force depending on the timescale for plasma decay. Theoretical and numerical analyses have shown that the expansion of dust clouds can fundamentally be different depending on which mechanism is dominant [2], [9]. A critical parameter in determining which expansion route occurs is the background neutral pressure [2]. At low neutral pressure, the plasma decays very quickly, and the shielding between the particles is greatly diminished. At high neutral pressure, the plasma decays on a longer timescale, and the frequent collisions between the electrons and the neutrals reduce the electron temperature which in turn causes a decrease in the dust charge. In this case, the screening of the particles remains effective, resulting in a much weaker dust cloud expansion [2]. Which process dominates in a particular experiment may sensitively depend on the initial conditions. By the initial conditions, we mean the size, shape, and density within the dust cloud, conditions which are difficult to reproduce from one experiment to another. No comprehensive analysis is yet available to distinguish which expansion process should apply for all of the cases presented in this paper. Furthermore, it is likely that a transition from one expansion regime to the other regime would occur.

Cases 1 and 2 (Section III-A, Fig. 2; and Section III-B, Fig. 3) showed similar dynamic evolutions in the plasma afterglow, although the initial clouds were quite different in size. The cloud in Case 1 had a volume that was roughly ten times that of cloud 2, so that it significantly contained more charge. Both clouds exhibited a blow-off of the outer layer of the lower portion of the cloud. For Case 2, a much larger layer was shed than in Case 1, and the density of the upper cloud continued to decrease over time. The cloud in Case 1 shed only a thin outer layer which expanded as it receded from the main cloud. The density in the main cloud remained unaffected for a much longer period of time compared with Case 2. The rate of separation of the outer layer was much higher in the l50 mTorr (Case 1) case. A rapid blow-off of the outer layer of a dust cloud is a characteristic of a Yukawa expansion, as shown in the theoretical work in [9]. A Yukawa expansion is also expected to be more likely at higher gas pressures, according to [2], although the MD simulations indicate that the transition from the Coulomb regime to the Yukawa regime occurs at a much higher pressure, 0.6 T, than the pressures used in the experiments.

As noted in Section III-E (Case 3), the observation of the Coulomb fission of a dust cloud was the most surprising result of this investigation. This differed qualitatively from Cases 1 and 2 in that the cloud splits into two separate clouds of comparable size, and each fragment maintained its identity. There is no theory of Coulomb fission of a dust cloud. We are performing a series of MD simulations [2], in which the initial cloud conditions are varied in an attempt to understand when one process might dominate over another. Coulomb fission of atomic clusters [10] and charged droplets [11] has been the subject of intensive theoretical and experimental investigation. The results of comparing the experimental observations with the MD simulations may reveal any common underlying physics between these two systems. For example, the breakup of charged droplets has been quantified in terms of the Rayleigh fissibility parameter $X = E(\text{Coulomb})/2E(\text{surface})$, where $E(\text{Coulomb})$ is the droplet Coulomb energy and $E(\text{surface})$ is the cluster surface energy which can be expressed in terms of the surface tension of the droplet [12]. It is not possible to apply this criterion to the dust cluster, because as yet there is no theory for the surface tension of a finite dust cluster.

Finally, we discuss Case 4 (Section III-E, Figs. 6 and 7) which was the only case in which we observed a simple expansion of a dust cloud, and can be compared with the theory. The cloud in Case 4 was not spherical in shape, but the dust within the cloud was symmetrically distributed about the center of the cloud, as can be seen in the dust density profiles in Fig. 6 at $t = 0$. The cloud then expanded uniformly, maintaining approximate Gaussian density profiles, as shown in Fig. 7. An analytical model for the expansion of a homogeneous charged sphere of the initial radius $r(0)$, containing dust particles each having a charge q_d and mass m_d, was presented in [9]. The initial dust number density was n_{d0}, and the particles were assumed to interact in pairs via a repulsive Coulomb potential. Neutral drag exerted on the particles by the ambient gas was included in the equation of motion for the individual spherical shells of the charged sphere. The confining potential for the spherical cloud was turned OFF at $t = 0$, and the motion of the shells of the Coulomb sphere dynamically evolved according to

$$\frac{d^2\rho}{d\tau^2} = \frac{1}{3\rho^2} - \frac{\gamma}{\omega_o}\frac{d\rho}{d\tau} \tag{1}$$

where $\rho = r/r_o$, $\omega_0 = (n_{d0}q_{d0}^2/\varepsilon_o m_d)^{1/2}$, $\tau = \omega_0 t$, and γ is the friction coefficient. As pointed out in [9], ω_0^{-1} represents a characteristic growth rate for the unstable (expanding) system. Fig. 7 (solid curve) shows the result of the numerical solution to (1) for $\omega_0 = 575\ \text{s}^{-1}$ and $\gamma = 330\ \text{s}^{-1}$, using the experimental values of n_{d0}, q_d, m_d, and $P_n = 26$ Pa. The value for the friction coefficient, γ, was obtained by measuring the terminal velocity, v_t, of dust particles under the action of gravity and neutral drag, where $v_t = g/\gamma$. The measured value for the friction coefficient is in agreement with the value obtained from the Epstein drag formula: $\nu_{Ep} = 4\pi\delta m_n n_n v_{Tn} a^2/3m_d$, where m_n is the mass of the neutral atoms, n_n is the neutral atom density, and v_{Tn} is the thermal speed of the neutrals, with the accommodation factor $\delta = 1.9$.

The agreement between the theoretical and experimental values is quite reasonable, considering the idealized nature of the model. This comparison is presented mainly to show that the expansion is most likely due to the repulsive Coulomb force between the dust particles. The deviation of the experimental data from the theoretical curve for $t > 10$ ms could be due to the fact that the model assumes a fixed charge, while the charge is probably decreasing as the expansion proceeds. The decrease in the dust charge for our conditions is related to the relaxation of the electron temperature due to electron–neutral collisions. Using the analysis in [5], we estimate that the time scale for electron temperature relaxation is $\sim$2 ms.

In summary, we have presented observations of the dynamics of dust clouds in an afterglow plasma. The results show a variety of outcomes from simple Coulomb expansion to Coulomb fission. The observed differences in behavior may indicate that the processes are sensitively dependent on the initial dust cloud configuration including its shape, the dust density, and location relative to the mesh. These observations were presented to stimulate further theoretical and numerical studies of how finite systems respond to a large excess charge. MD simulations of dust cloud evolution in afterglow plasmas are currently underway, and the results will be presented in a future publication.

REFERENCES

[1] A. Barkan and R. L. Merlino, "Confinement of dust particles in a double layer," *Phys. Plasmas*, vol. 2, no. 9, pp. 3261–3265, 1995.

[2] V. Saxena, K. Avinash, and A. Sen, "Dust cluster explosion," *Phys. Plasmas*, vol. 19, no. 9, pp. 093706-1–093706-5, 2012.

[3] I. I. Filatova, F. M. Trukhachev, and N. I. Chubrik, "Study of the process of dust grain discharging in the afterglow of an RF discharge," *Plasma Phys. Rep.*, vol. 37, no. 12, pp. 1042–1045, Dec. 2011.

[4] T. Antonova *et al.*, "Microparticles deep in the plasma sheath: Coulomb 'explosion,"' *Phys. Plasmas*, vol. 19, no. 9, pp. 093709-1–093709-6, 2012.

[5] A. V. Ivlev *et al.*, "Decharging of complex plasmas: First kinetic observations," *Phys. Rev. Lett.*, vol. 90, pp. 055003-1–055003-4, Feb. 2003.

[6] L. Couëdel, M. Mikikian, L. Boufendi, and A. A. Samarian, "Residual dust charges in discharge afterglow," *Phys. Rev. E*, vol. 74, pp. 026403-1–026403-9, Aug. 2006.

[7] L. Couëdel, A. A. Samarian, M. Mikikian, and L. Boufendi, "Dust charge distribution in complex plasma afterglow," *Europhys. Lett.*, vol. 84, no. 3, pp. 35002-1–35002-5, Oct. 2008.

[8] A. V. Ivlev, "Coulomb expansion: Analytical solutions," *Phys. Rev. E*, vol. 87, pp. 025102-1–025102-3, Feb. 2013.

[9] A. Piel and J. A. Goree, "Collisional and collisionless expansion of Yukawa balls," *Phys. Rev. E*, vol. 88, pp. 063103-1–063103-11, Dec. 2013.

[10] Y. Levy, I. Last, and J. Jortner, "Dynamics of fission and Coulomb explosion of multicharged large finite systems," *Molecular Phys.*, vol. 104, no. 8, pp. 1227–1237, 2006.

[11] J. C. Burton and P. Taborek, "Simulations of Coulombic fission of charged inviscid drops," *Phys. Rev. Lett.*, vol. 106, pp. 144501-1–144501-4, Apr. 2011.

[12] I. Last, Y. Levy, and J. Jortner, "Beyond the Rayleigh instability limit for multicharged finite systems: From fission to Coulomb explosion," *Proc. Nat. Acad. Sci. USA*, vol. 99, no. 14, pp. 9107–9112, 2002.

John K. Meyer received the Ph.D. degree in physics from The University of Iowa, Iowa City, IA, USA, in 2015. His thesis work was involved in experimental plasma physics on Experiments in Flowing and Freely Expanding Dusty Plasmas.

He is currently a Post-Doctoral Fellow with Forschungsgruppe Komplexe Plasmen, Deutsches Zentrum für Luft- und Raumfahrt, Weßling, Germany.

Robert L. Merlino received the Ph.D. degree in physics from the University of Maryland, College Park, MD, USA, in 1980.

He is currently a Professor of Physics with the Department of Physics and Astronomy, The University of Iowa, Iowa City, IA, USA. His current research interests include basic plasma physics and dusty plasmas.